



Integrated petrophysical and petrographical studies for characterization of reservoirs: a case study of Muglad Basin, North Sudan

Abeer A. Abuhagaza¹ · Marwa Z. El Sawy¹ · Bassem S. Nabawy²

Received: 2 May 2020 / Accepted: 4 February 2021 / Published online: 20 February 2021
© The Author(s), under exclusive licence to Springer-Verlag GmbH, DE part of Springer Nature 2021

Abstract

Petrography, scanning electron microscopy, X-ray diffraction, and both conventional and special core analyses are applied to precisely reservoir characterize the Lower Cretaceous Bentiu and Abu Gabra Formations of the Muglad Basin, which is among the largest hydrocarbon reservoirs in South Kordofan, SW North Sudan. Based on this integrated study, the Abu Gabra–Bentiu sequence comprises four petrographical microfacies, which consist of two reservoir rock types (RRTs). RRT1 is composed of quartz arenites and RRT2 is composed of quartz wackes. The greatest storage, flow capacities, and reservoir quality are assigned for RRT1 due to its good-to-excellent porosity (average $\varnothing = 26.7\%$), permeability (average $k = 1365$ md), reservoir quality index (RQI, average = $1.43 \mu\text{m}$), flow zone indicator (FZI, average = $3.66 \mu\text{m}$) and discrete rock type (DRT, average = 13). The relatively low-to-fair reservoir quality of the Abu Gabra Formation (average $\varnothing = 13.2\%$, average $k = 14.7$ md, average RQI = $0.17 \mu\text{m}$, average FZI = $1.05 \mu\text{m}$, and average DRT = 10) is due to authigenic kaolinite and siderite content, compaction and cementation by silica and clay patches.

Keywords North Sudan · Muglad Basin · Petrophysics · Reservoir quality · Abu Gabra · Bentiu

List of symbols

RRT	Reservoir rock type	FZI	Flow zone indicator
HFU	Hydraulic flow unit	RPI	Reservoir potentiality index
\varnothing_{He}	Helium porosity	SEM	Scanning electron microscopy
\varnothing_{SF}	Summation fluid porosity	XRD	X-ray diffraction
k_{H}	Horizontal gas permeability	m	Porosity exponent
k_{V}	Vertical gas permeability	a	Lithology factor
DRT	Discrete rock type	m'	Porosity exponent at overburden pressure
ρ_{b}	Bulk density	a'	Lithology factor at overburden pressure
ρ_{g}	Grain density	λ_k	Permeability anisotropy
RQI	Reservoir quality index	V	Heterogeneity index of Dykstra-Parsons
NPI	Normalized porosity index	Ro	Apparent electric resistivity
		Rt	True electric resistivity
		Rw	Water resistivity
		RI	Resistivity index
		FRF	Formation resistivity factor
		Sw_{irr}	Irreducible water saturation
		PR	Pore volume reduction
		PTHR	Pore throat reduction
		k_{ro}	Relative permeability to oil
		k_{rw}	Relative permeability to water
		QFL	Quartz–feldspars–lithic fragments triangle

✉ Bassem S. Nabawy
bsnabawy@yahoo.co.uk

Abeer A. Abuhagaza
abeerahmed@epri.sci.eg

Marwa Z. El Sawy
marwa_epri@yahoo.com

¹ Department of Exploration, Egyptian Petroleum Research Institute, Cairo, Egypt

² Department of Geophysical Sciences, National Research Center, Cairo, Egypt

Introduction

The Muglad Basin is a main part of the Cretaceous rift system that extends through the central and western African rift system. Its tectonic situation is controlled by a series of regional faults and fracture zones exhibiting disparate trends. The structural systems of this basin are dominated by faults trending from the northwest to the southeast parallel to the basin axis (Fairhead 1988; Schull 1988; McHargue et al. 1992).

The mineralogical composition of sedimentary rocks reflects the effects of geological provenance, sedimentary environment and diagenetic processes (Raymond 2002). Reservoir properties are determined primarily by mineral composition and the dominant diagenetic factors of the reservoir sequence. Reservoir petrophysical analysis can be used to characterize reservoirs and classify different

pore types (De Ros and Goldberg 2007; Kassab et al. 2017a).

The present study was primarily aimed at estimating the dominant reservoir conditions of the Bentiu and Abu Gabra Formations in block-4 of the Muglad Basin (Fig. 1). This was achieved by interpreting the results of petrographical, scanning electron microscopy (SEM), and X-ray diffraction (XRD) analyses of the studied sequence in addition to available routine and special core data.

Useful reservoir modeling requires some details on the mineral composition of the studied sequence and the impacts of relevant dominant diagenetic factors. The reservoir sequence rock types should also be described based on their mineral compositions.

In addition, wettability can be predicted using two relative permeability methods and then compared with the Amott technique to evaluate their reliability. Integration between results can provide the volumetric parameters of sandstone

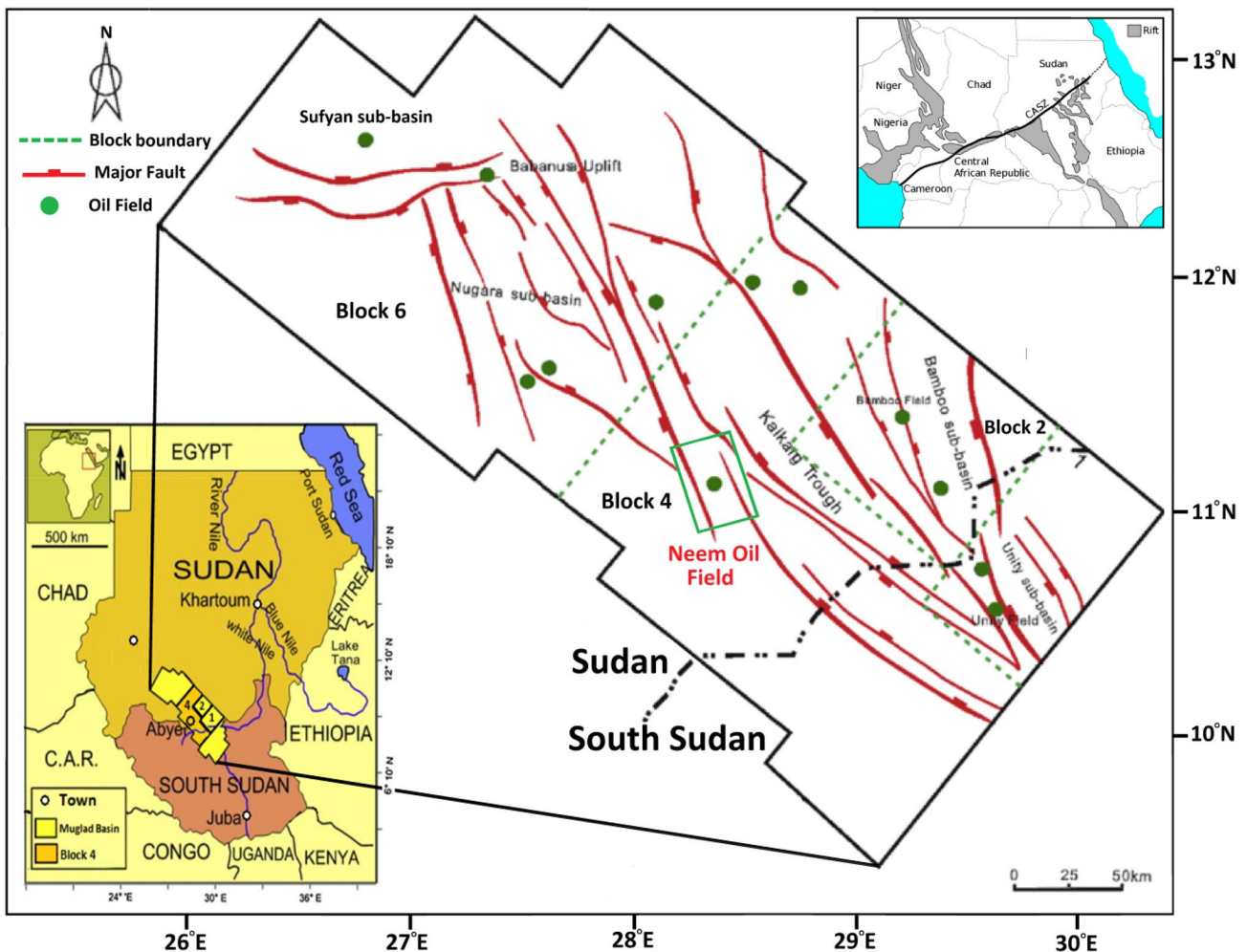


Fig. 1 Geologic map of the southern part of the Sudan indicating the location of Neem oil field in block 4. CASZ trend in the map at the top right corner is the Central African Shear Zone. The grey colour

refers to the main rift systems in Sudan and the central parts of Africa (modified after Makeen et al. 2016; El Sawy et al. 2020).

reservoirs and their response to different petrophysical and sedimentological properties. Measurements of electric resistivity are considered an important tool to estimate the values of porosity exponent, m , tortuosity factor ‘ a ’, and saturation exponent, n , of Archie (1942), each of which are valuable when evaluating porosity and hydrocarbon reserves.

Lithostratigraphy and depositional environments

The Muglad Basin is composed of thick continental, non-marine clastic sequences of Late Jurassic to Early Cretaceous sediments from surrounding uplifted regions and is rich in hydrocarbon resources (El Hassan et al. 2017). The basin terminates in its northwestern section by the Central African Shear Zone, CASZ (Schull 1988; Fairhead 1988; McHargue et al. 1992).

The lithostratigraphic column of block-4 in Muglad Basin can be subdivided into three depositional cycles (Fig. 2,

Abdalla et al. 2002; Abdelhakam and Ali 2008). The first rift cycle, which dates to the Early Cretaceous age, consists of organic-rich lacustrine shales that form the main source beds of the Abu Gabra Formation (Qiao et al. 2016). These shales are overlain (in the sag phase) by coarse- to medium-grained sandstones of the Bentiu Formation. The second Late Cretaceous–Paleocene cycle begins with deposition of the Darfur Group, which is composed of deltaic and fluvial claystones of the Aradeiba Formation at the base, and thin sandstone beds of the Ghazal and Zarqa Formations. The sandstone beds increases in thickness up to the Baraka Formation near the top of this cycle and are overlain by coarse clastics of the Amal Formation (Lowell and Genik 1972). The third depositional cycle is represented by the Oligocene–Late Eocene Kordofan Group, which consists of the shaly Tendi and Nayil Formations, in addition to the Adok coarse-grained sandstones. The top of the section is composed of the Miocene–Holocene Zeraf Formation, which unconformably overlies the fluvial deposits of the Adok Formation.

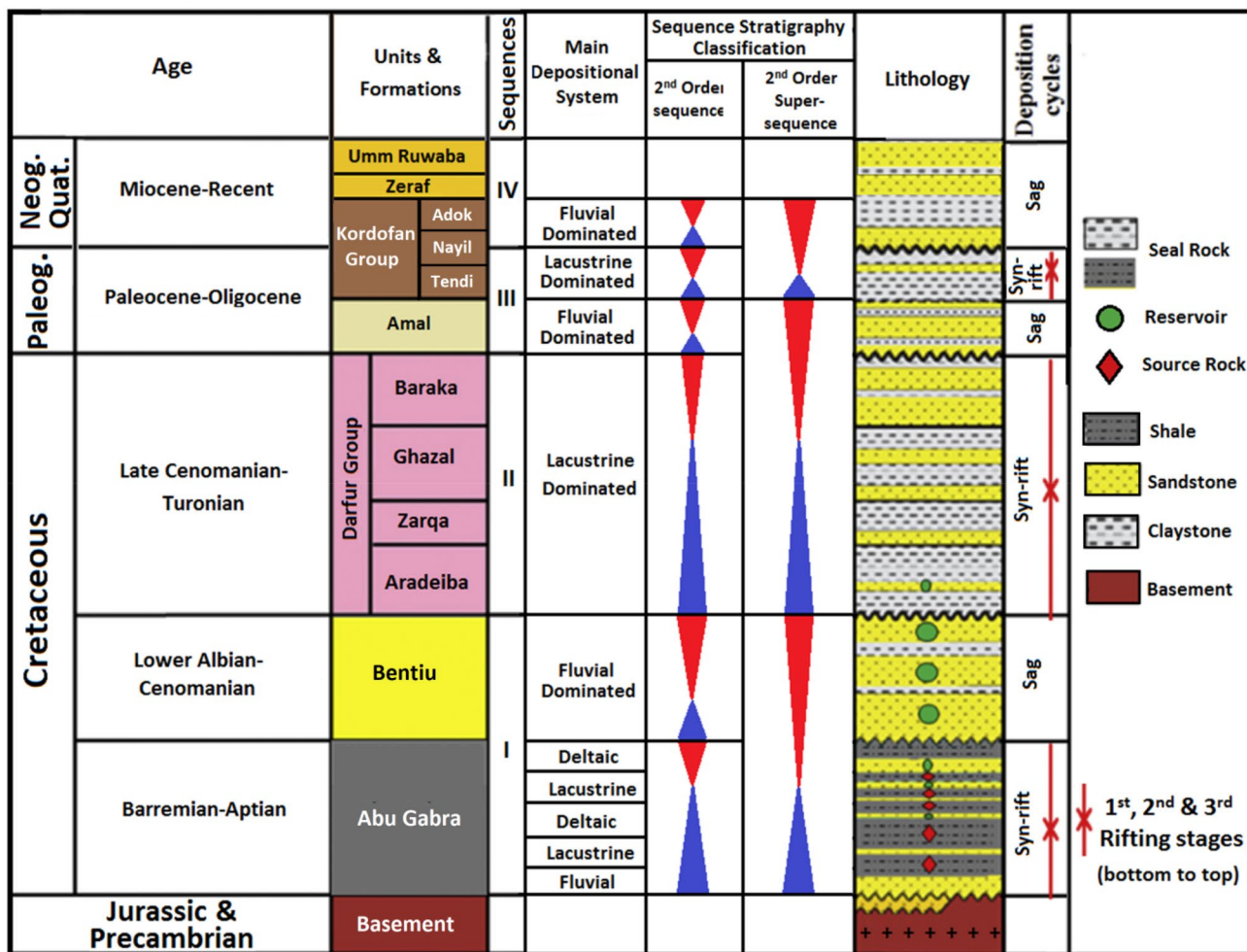


Fig. 2 Regional stratigraphy of the Muglad Basin (Schull 1988; Dou et al. 2013; Makeen et al. 2016)

The Abu Gabra Formation is the main proven source and reservoir rock sequence in the Muglad Basin. It consists of lacustrine shale and mudstone, approximately 2000 m thick, with a high amount of organic matter consisting of a wide cap rock at the depocenter and characterized by interbedded sands that produce condensate, light oil and considerable volumes of associated and dry gas. The net-pay reservoir thickness in Abu Gabra may reach up to 15 m thickness of deltaic facies. The Bentiu Formation represents the second reservoir interval in the Muglad Basin with 10 m of total net-pay of a blocky sandstone sequence of fluvial facies (Dou et al. 2006).

Methods

The mineral composition and dominant diagenetic factors of the studied formations were examined in detail using a representative number of blue-dyed thin sections, scanning electron microscopy (SEM) images, and X-ray diffraction (XRD) data. The studied selected clastic samples were classified according to the quartz, feldspar and lithic fragments, (QFL) triangle of Pettijohn et al. (1987).

For petrophysical studies, a full set of conventional core analyses (bulk and grain densities (ρ_b and ρ_g , respectively), helium and summation fluids porosities (\varnothing_{He} and \varnothing_{SF} , respectively), vertical and horizontal permeabilities (k_v & k_H , respectively), as well as water and oil saturations (S_w and S_o , respectively), was applied to the samples (Table 1). Full description for these methods provided by (Nabawy and El Sharawy 2015; Nabawy et al. 2018a, b).

To estimate the reservoir quality of the studied sequence, the reservoir quality index (RQI, in μm), normalized porosity index (NPI, in fractions), flow zone indicator (FZI, in μm) and reservoir potentiality index (RPI) were applied (Table 1) as recommended previously (e.g., Amaefule et al. 1993; Tiab and Donaldson 1996; Corbett

and Potter 2004; Teh et al. 2012; Abed 2014; Kassab et al. 2017b; Nabawy et al. 2018b, 2020; Elgendy et al. 2020). The reservoir quality parameters were calculated as follows:

$$FZI = \frac{RQI}{NPI} \quad (\text{Amaefule et al.1993}), \tag{1}$$

$$RQI = 0.0314 \sqrt{\frac{k}{\varnothing}} \quad (\text{Amaefule et al. 1993}), \tag{2}$$

$$NPI = \frac{\varnothing}{1 - \varnothing} \quad (\text{Amaefule et al. 1993}), \tag{3}$$

where k is permeability (in md), and \varnothing is porosity (in decimals).

Nabawy et al. (2018b) introduced classification ranks for both the RQI and FZI, and the RPI (rank parameter) was then estimated as the arithmetic mean of the ranks obtained for both the RQI and the FZI as follows.

$$RPI = \frac{RQI_{rank} + FZI_{rank}}{2} \quad (\text{Nabawy et al.2018b}) \tag{4}$$

Discriminating the studied samples into rock types can be supported by applying the discrete rock type technique of Shenawi et al. (2007) who proposed a mathematical model for combining samples with similar petrophysical properties into similar DRT numbers as follows.

$$DRT = \text{ROUND} (2 \times \text{Ln}(FZI) + 10.6;0) \tag{5}$$

(Shenawi et al.2007; El Sharawy and Nabawy 2018)

Reservoir zonation into a number of hydraulic flow units were applied by summing depths with the same reservoir ranks into one flow unit, after which the stratigraphic modified Lorenz technique was applied (Maglio-Johnson 2000).

Table 1 Storage capacity data and the reservoir quality parameters of the studied Neem north-2 well, block-4, southeast Muglad Basin, Sudan

RRT	Facies		ρ_b g/cm ³	ρ_g g/cm ³	\varnothing_{He} %	\varnothing_{SF} %	k_H md	k_v md	λ_k 0.00	S_w %	S_o %	RQI μm	NPI 0.00	FZI μm	RPI 0.00	DRT 0.00
RRT-1 (43 plugs)	Quartz arenites	Min	1.740	2.634	19.97	16.42	138.2	41.49	1.20	19.20	19.20	0.61	0.25	2.37	3.0	12.0
		Max	2.122	2.659	34.07	32.71	4140	2074	3.69	51.10	55.20	2.91	0.52	6.12	5.0	14.0
		Mean	1.940	2.645	26.68	22.52	1365	489.9	1.95	28.10	43.56	1.43	0.37	3.66	4.0	13.0
RRT-2 (17 plugs)	Quartz wackes	Min	2.062	2.628	4.28	3.10	0.06	0.09	0.30	41.70	0.00	0.04	0.04	0.53	0.0	9.0
		Max	2.639	2.765	22.38	19.02	69.31	29.18	2.41	75.60	43.29	0.42	0.29	1.94	1.0	11.0
		Mean	2.324	2.676	13.22	11.06	14.65	4.77	1.38	57.63	17.86	0.17	0.16	1.05	1.0	10.0

ρ_b and ρ_g are the bulk and grain densities, respectively; \varnothing_{He} and \varnothing_{SF} are the helium and summation fluids porosities, respectively; k_H and k_v are the horizontal and vertical air permeabilities, respectively; λ_k is the anisotropy of permeability; S_w and S_o are the water and oil saturations, respectively; RQI and NPI are the reservoir quality and normalized porosity indices, respectively; FZI and RPI are the flow zone indicator and the reservoir potentiality index, respectively; and DRT is the discrete rock type in digits

Permeability anisotropy (λ_k) was also calculated as recommended previously (Serra 1988; Nabawy et al. 2018b; Nabawy 2018):

$$k = \sqrt{\frac{k_H}{k_V}} \quad (\text{Serra 1988}). \quad (6)$$

Reservoir heterogeneity (V) was estimated using the Dykstra–Parsons technique (Dykstra and Parsons 1950), and classified following El Sharawy and Nabawy (2018) into an extremely heterogeneous reservoir ($1.0 \geq V > 0.75$), a highly heterogeneous reservoir ($0.75 \geq V > 0.50$), a moderately heterogeneous reservoir ($0.50 \geq V > 0.25$), a slightly heterogeneous reservoir ($0.25 \geq V > 0.10$), and a homogeneous reservoir ($0.10 \geq V$).

To estimate the porosity exponent (m) and lithology factor (a) of Archie’s equation (Archie 1942), the apparent electric resistivity (R_o) of fully-saturated plug samples (water resistivity $R_w = 0.653 \Omega \text{ m}$), and the formation resistivity factor ($FRF = R_o/R_w$) were measured. Archie’s parameters (Archie 1942) were estimated.

$$FRF = a / \phi^m \quad (7)$$

To determine the impacts of increase pressure on the electric properties and Archie’s parameters (a and m), the FRF of some selected samples was measured at 4300 psi of confining pressure.

In addition, the irreducible water saturation (Sw_{irr}) was measured using the porous plate method at different pressures (1–200 psi), and the water saturation was measured at each applied pressure. The electric resistivity was measured at 100% saline saturation (R_o). The true electric resistivity (R_t) was measured at each step of decreasing water

saturation and the resistivity index (RI) was calculated as $RI = R_t/R_o$ until it reached the Sw_{irr} . Plotting RI values as a function of Sw values enabled estimation of the saturating exponent, n of Archie’s equation (1942).

To determine the impacts of an incremental increase in the applied pressure on the reservoir properties, porosity and permeability of nine samples were measured at ambient conditions and incremental increasing confining pressures (14.5, 400, 1000, 1500, 2000, 3000, 4000, 5000, and 6000 psi) (Table 2). The pore volume reduction (PR) and the pore throat reduction (PTHR) were then measured as follows:

$$PR = 100 \times (\phi_{14.5} - \phi_{6000}) / \phi_{14.5}, \quad (8)$$

$$PTHR = 100 \times (k_{14.5} - k_{6000}) / k_{14.5}, \quad (9)$$

where $\phi_{14.5}$, ϕ_{6000} , $k_{14.5}$, and k_{6000} are the measured porosity and permeability at 14.5 and 6000 psi, respectively.

The relative permeability to oil and water (k_{ro} and k_{rw}) of some samples was measured using a water–oil flushing system, with the results plotted as a function of Sw . The obtained curves were used to determine the wettability of samples, which were ranked as neutral, weak, moderate, and strongly oil or water wet according to a classification proposed by Nabawy et al. (2018b). It is based on the relative permeability index which can be calculated as follows.

$$\text{Wettability index} = 2 \times (0.5 - krw_{max}), \quad (10)$$

where krw_{max} is the max water relative permeability.

In addition, the Amott technique was applied as a direct measure for wettability.

Table 2 Porosity and permeability values of some RRT1 samples at an ambient pressure of 14.5 psi and at overburden pressures of 400, 1000, 1500, 2000, 3000, 4000, 5000 and 6000 psi

	Porosity (%)								PR %
	14.5	400	1000	1500	2000	3000	4000	6000	
Min	12.6	11.2	10.8	10.6	10.5	10.4	10.2	10.2	13.6
Max	31.4	27.2	26.7	26.2	25.8	25.4	24.9	24.5	22.6
Mean	26.0	23.0	22.6	22.2	21.9	21.6	21.3	21.0	19.3
	Permeability (md)								PTHR %
	14.5	400	1000	2000	3000	4000	5000	6000	
Min	163	81.3	77.8	69.6	64.7	61.4	59.3	57.2	31.34
Max	3974	2412	235	2166	2066	1998	1946	1905	47.94
Mean	1010	610	567	518	491	473	460	449	39.62

PR pore reduction, PTHR pore throat reduction

Results

Microfacies analysis

Plotting data of the petrographic examination of both the Bentiu and Abu Gabra Formations on QFL triangle enabled discrimination of the selected sandstone samples into four microfacies (Fig. 3): quartz arenite, quartz wacke, subfeldspathic quartz arenite and subfeldspathic wacke microfacies.

Quartz arenite

Most of the studied interval of the Bentiu Formation is composed of moderately to poorly sorted, subrounded to subangular, very fine to very coarse quartz grains cemented by patchy kaolinite and pore-filling booklets. Silica cement (Fig. 4a) and subordinate quantities of ferruginous patchy and pore-filling siderite cement are also present, which slightly reduced the pore spaces (Fig. 4b). Quartz grains are moderately compacted, with sutured, long, pointed and concavo-convex contacts (Fig. 4a). Moderate-to-good pore interconnectivity of the quartz arenite samples with primary interparticle and secondary oversize pores are the products of leaching some clay matrix and partial to complete dissolution and leaching out of feldspars. The presence of microfractures in some quartz grains slightly enhanced the porosity of a few plug samples (Fig. 4a, b).

Quartz wacke

Quartz wacke microfacies recorded in some intervals of the Bentiu and Abu Gabra Formations is composed of poorly sorted, subrounded to subangular, very fine to coarse-grained quartz, cemented mostly by silica cement and clay patches (Fig. 4e) with limited amounts of alkali feldspars, mica flakes and carbonaceous material (Fig. 4d, e). Types of pore spaces and a precise value of visual porosity could not be estimated easily due to filling of the pore spaces by silica cement and clay matrix (Fig. 4e). However, porosity is mostly represented by intergranular and vuggy pore spaces, partially filled with cement.

Subfeldspathic quartz arenite

Subfeldspathic quartz arenite microfacies is found primarily in Abu Gabra Formation and consists of quartz grains with some partially to completely altered alkali feldspars floating in siliceous and ferruginous cement (Fig. 4g, f). The quartz grains are subangular to subrounded, moderately sorted, sometimes of medium size, and sometimes forming thin lamina of fine-grained quartz grains of long and pointed grain contacts (Fig. 4g). The porosity of the subfeldspathic quartz arenite samples is fair to good (10–20% vol.), represented largely by intergranular and oversized pore spaces due to cement dissolution. Siliceous and ferruginous cement materials reduced the interconnected pore volume to poor values (Fig. 4f, g).

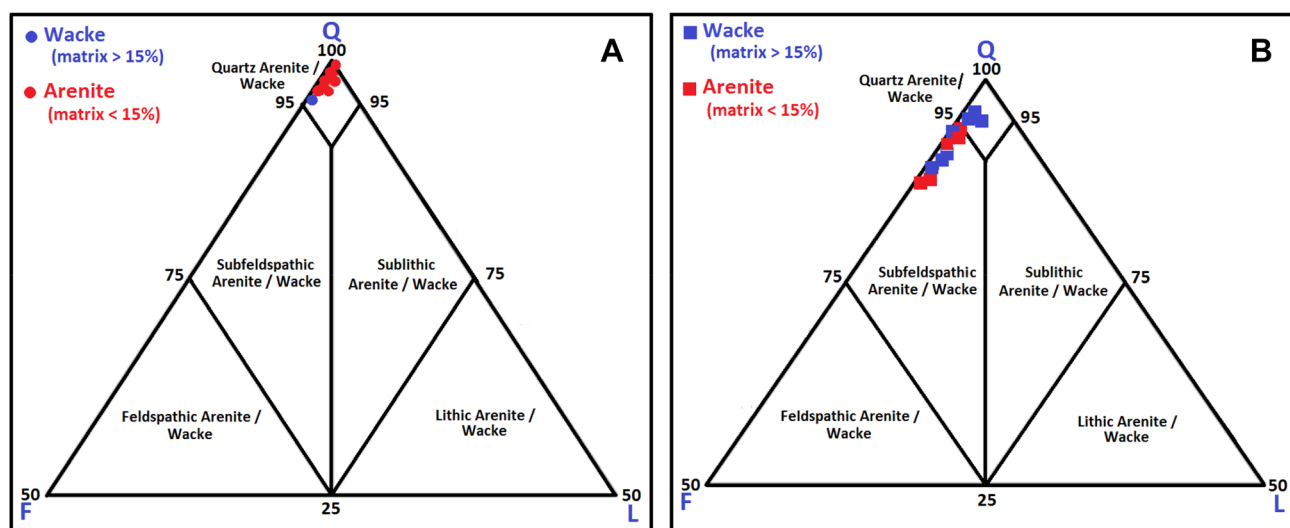


Fig. 3 Ternary diagram (QFL) of Pettijohn et al. (1987) showing the framework compositions and classification of: **a** Bentiu Formation, and **b** Abu Gabra Formation. *Q* quartz, *F* feldspar, *L* rock fragments

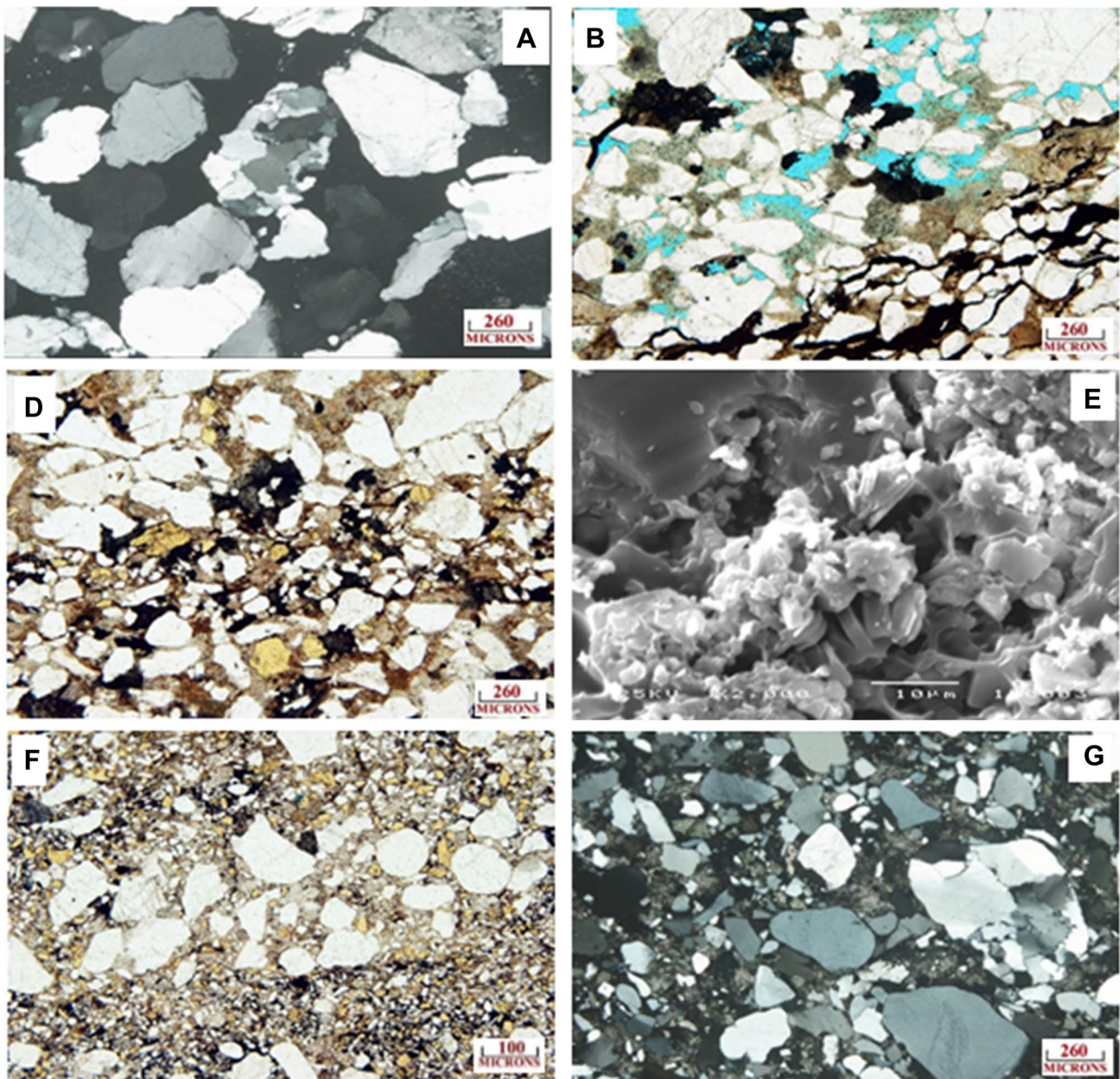


Fig. 4 Photomicrographs and SEM results of the Bentiu and Abu Gabra Formations showing: **a** very fine to very coarse monocrystalline quartz grains quartz with subordinate quantities of polycrystalline grains, and quartz arenite microfacies at a depth of 1862.03 m, **b** fine to coarse quartz grains cemented by ferruginous cement and quartz arenite at a depth of 1866.78 m, **c** SEM photomicrograph showing dissolution of quartz grains with minor microcrystalline siderite, and pyrite crystals, quartz arenite microfacies, at depth

1868.77 m, **d** SEM photomicrograph showing common well-crystallized patchy pore-filling kaolinite booklets due to quartz and feldspar dissolution, and subfeldspathic arenite microfacies, at depth 2192.00 m, **e** very fine to coarse quartz grains with common alkali feldspar cemented by argillaceous and ferruginous materials, subfeldspathic wacke, at a depth of 2186.5 m, and **f** poorly sorted subfeldspathic wacke with subordinate quantities of polycrystalline quartz, at a depth of 2192.65 m

Subfeldspathic wacke

Petrographically, the subfeldspathic wacke microfacies is composed of ill-sorted, very fine to coarse-grained, rounded to subangular quartz grains, which are poorly compacted with little alkali feldspars. They are mainly cemented by

argillaceous cement materials that greatly reduced the pore spaces. The visual porosity of this microfacies is not easily estimated, as it is represented by micro-intergranular pore spaces that are greatly reduced and diminished due to cementation and mechanical infiltration of clays from the beds above (Fig. 4f, g).

Diagenetic factors

The studied samples were affected by a series of diagenetic cycles that have strong influence on porosity and permeability. Following Nabawy et al. (2020), the diagenetic processes controlling the petrophysical properties of the present samples were sorted into a number of factors that enhanced or reduced reservoir quality as follows:

Reservoir quality-reducing diagenetic processes

Compaction and pressure solution: Packing of framework grains due to increasing stress effects in the sandstones of both the Bentiu and Abu Gabra Formations indicates that all the studied samples are poorly to moderately compacted. Mechanical compaction can be indicated by the presence of microfractures in quartz and feldspar grains (Fig. 4a). Chemical compaction exerts pressure dissolution along the grain contacts because of dominant physical compaction that is declared by different grades of fractured grains compacted together in pointed, long, concave-convex and straight contacts (Fig. 4a, h). The compaction process reduced the interstitial pore space and increased the percentage of long and sutured contacts between the framework grains and precipitation of new cement materials.

Cementation: Silica is the dominant cement materials in the studied sandstone samples of both the Bentiu and Abu Gabra Formations, reducing intergranular pore spaces. It is mostly represented by a quartz overgrowth pressure solution causing greater grain-to-grain compaction and authigenic microcrystalline quartz (Fig. 4a). Carbonate cement in the form of ferroan calcite and siderite patches, is rarely present in the studied samples (Fig. 4g), and was mostly dissected by precipitation of later siliceous cement. A few ferruginous cement patches and pore-filling kaolinite are recorded in some samples filling the intergranular pores.

Authigenic minerals: Kaolinite is the dominant authigenic clay mineral in the studied samples due to alteration of feldspar grains and mica flakes. Authigenic vermicular stacks and booklets of kaolinite are present as filling materials for pores (Fig. 4e, h). Well-developed syntaxial quartz overgrowths are evident in most samples (Fig. 4e). Siderite and pyrite was recorded in some samples as patchy rhombic and subcubic crystals filling pores and locally replacing detrital clays.

Reservoir quality-enhancing diagenetic processes

Dissolution and leaching: Dissolution in clastic rocks has been documented as a promoting factor that creates a secondary porosity and enhances reservoir characteristics. For

the Bentiu and Abu Gabra samples, dissolution of feldspars is indicated by the presence of altered feldspar relics as well as some authigenic kaolinite booklets (Fig. 4e).

Fracturing: Fracturing is a leading process that increases secondary porosity by adding extra fracture pores, which are evident in the studied samples in the form of fractured quartz grains of the arenite microfacies (Fig. 4b). The existence of different sets of intersecting micro-fracture sets helps in creating a pore network with high degree of connectivity which increases the ability of dissolving fluids to invade rocks and enhance their enhancing impacts on reservoir quality.

Mineralogy using XRD analysis

Semi-quantitative results of the analyzed Bentiu and Abu Gabra samples show that quartz is the most abundant mineral (67.1–95.3% vol.) with minor amounts of feldspars (up to 10.7% vol.), although the amounts are greater in Abu Gabra Formation. This is in addition to trace amounts of calcite and dolomite (up to 2.41% vol.), and siderite (up to 7.92% vol.). Kaolinite reaches 13.97% vol. in the Abu Gabra and increases upward in the Bentiu Formation, reaching up to 18.3% vol. Cement materials (calcite, dolomite and siderite) and the clay matrix (kaolinite, chlorite, and illite) increases upward through the Abu Gabra Formation and reaches their maximum values at the top and bottom of the Bentiu Formation as shown in the vertical variation of mineralogical composition (Fig. 5). Increasing the kaolinite content upward in the Abu Gabra and Bentiu Formations indicates a tropical continental setting with kaolinite mineral dominant in near-shore regions (Mousa et al. 2014).

Petrophysical results

The four petrographical microfacies were summed up petrophysically into two reservoir rock types (RRTs), each with its diagnostic petrophysical behavior and reservoir quality.

Routine and special analysis data of the studied rock types are listed and discussed in details the following section.

RRT1

This rock type is composed primarily of quartz arenite and subfeldspathic quartz arenite and is dominated by quartz grains. It represents samples of the Bentiu Formation and a few samples from the Abu Gabra Formation. Petrophysical properties of the RRT1 samples are listed in Tables 1, 2 and 3.

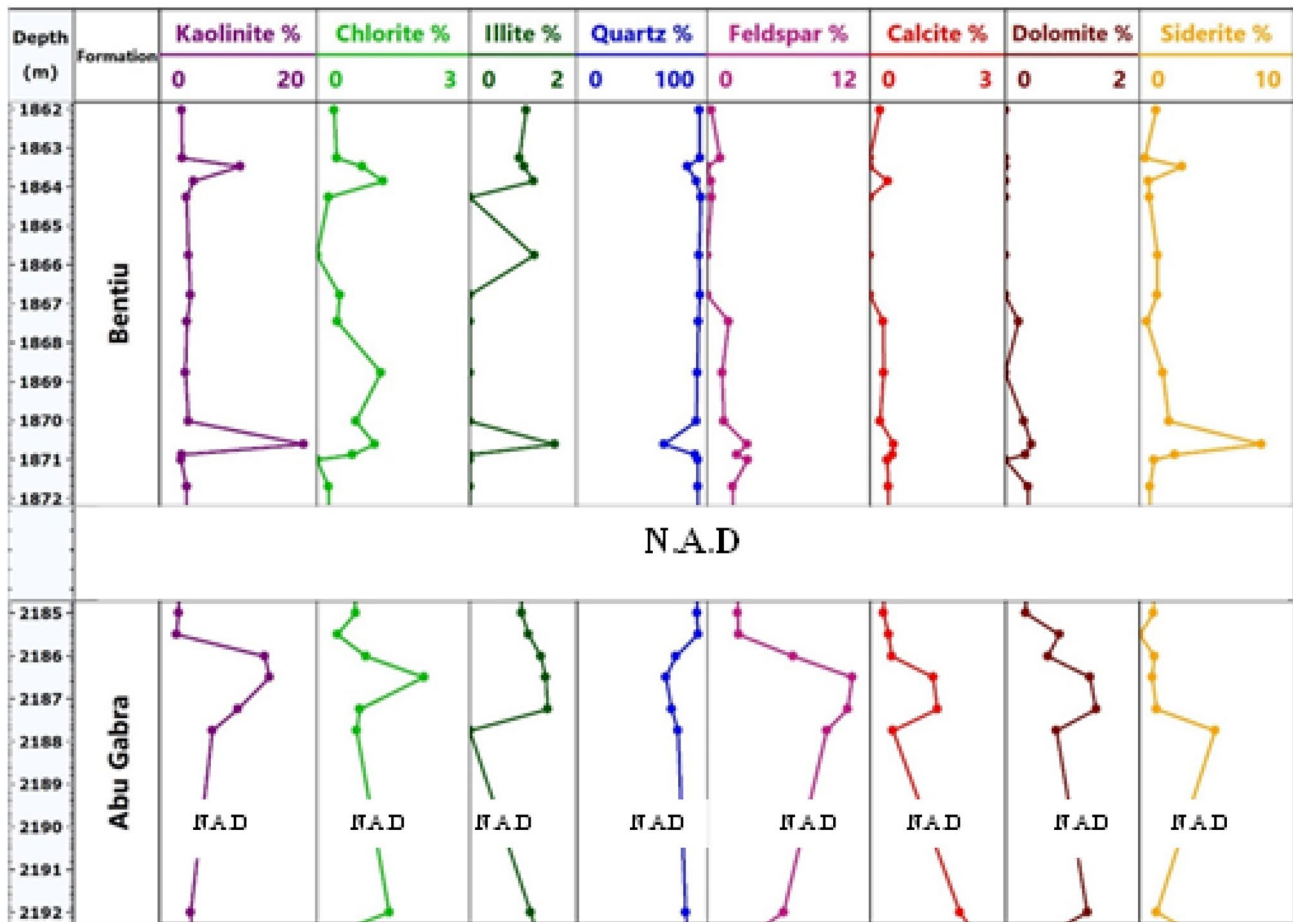


Fig. 5 Vertical variation of mineralogical composition from XRD analysis of the Bentiu and Abu Gabra Formations. *NAD* not available data

Table 3 Relative permeability values for both oil and water in the studied Bentiu RRT1 samples estimated using the common intersection method and the new proposed method as shown in Fig. 15, in addition to the Amott index method

S. no.	RPIP %	Wettability	kr index	Wettability	Amott index	Wettability
1	66.3	Water wet	0.55	Weakly water wet	0.689	Moderately water wet
2	52.0	Water wet	0.40	Weakly water wet	0.569	Weakly water wet
3	35.4	Oil wet	0.14	Neutral	0.409	Weakly water wet
4	54.1	Water wet	0.48	Weakly water wet	0.600	Weakly water wet
5	55.6	Water wet	0.54	Weakly water wet	0.662	Moderately water wet
6	47.1	Oil wet	0.18	Neutral	0.428	Weakly water wet

RPIP is the relative permeability intersection point, which is equal to the water saturation value that corresponds to the intersection point between the relative permeability curves of both water and oil; and *kr* index is the relative permeability index

RRT2

Samples of RRT2 are composed mostly of subfeldspathic wacke and quartz wacke which indicates a partial dominance of clay patches. This RRT represents most samples

of the Abu Gabra Formation and few samples from Bentiu Formation.

Increasing the clay matrix in addition to the calcareous, ferruginous and siliceous cementation of the wacke samples decreased their reservoir potentiality. Values of

the measured petrophysical parameters of RRT2 samples are listed in Tables 1, 2 and 3.

Discussion

Data quality assurance

An absence of rugosity and roughness of the plug samples is an important criteria that can provide a precise estimating of plug volume, i.e., their petrophysical properties, and reservoir quality. Quality assurance for the bulk volume of samples is achieved by plotting porosity (\varnothing_{He}) as a function of bulk density (ρ_b) (David et al. 2015; Nabawy et al. 2020) (Fig. 6). The resulting plot indicates a high reliability of the obtained mathematical models with high determination coefficient ($R^2 = 0.990$). In addition, this plot indicates successful separation of the studied plugs into two rock types using 20% porosity as a separating value between the two types.

Porosity (\varnothing_{He}) contribution to permeability (k)

Horizontal permeability values (k_H) were plotted as a function of porosity (\varnothing_{He}) to measure the contribution of porosity to flow capacity (Fig. 7). The obtained $k - \varnothing$ mathematical models are characterized by high reliability ($R^2 \geq 0.799$). The obtained trend lines support

discrimination of the studied data into two RRTs. The RRT1 samples are characterized by moderate DRT values (9–11), whereas the RRT2 samples exhibited higher DRT values (12–14, Fig. 7). DRT values are based on FZI values, i.e., they indicate reservoir quality, the higher the DRT values, the better the reservoir quality.

In general, reservoir quality parameters are direct measures of the contribution of porosity to reservoir permeability. Following a classification ranking scale introduced by Nabawy et al. (2018b), RQI plotted as a function of FZI indicated fair to very good RQI values ($0.5 \leq \text{RQI} \leq 5.0 \mu\text{m}$) and poor to good FZI values ($1.0 \leq \text{FZI} \leq 10.0 \mu\text{m}$, Fig. 8).

Plotting k_V as a function of k_H (Fig. 9) indicates that the RRT1 samples are dominated by depositional fabrics (foliated fabrics) due to presence of altered feldspars and relics of formerly leached out clay content that created some foliated pore spaces. Some vertical permeability values are higher than the horizontal permeability values, which can be explained by the presence of a subsidiary micro-fracture system (Fig. 4b). This plot is supported by Fig. 10, in which the vertical and horizontal permeability relationship is supported by a scale for measuring permeability anisotropy (λ_k), which can be calculated using Eq. (6). Figure 10 shows that most of the RRT1 samples could be characterized by moderately depositional fabrics ($1.5 < \lambda_k \leq 2.5$), with a few slightly and highly anisotropic samples. By comparison, samples of RRT2 are characterized by the presence of highly to slightly secondary fabrics, while the others are moderately to slightly depositional fabrics. This indicates dominance of

Fig. 6 Plotting helium porosity as a function of bulk density for different rock types, Neem North-2 well, block-4, SE Muglad Basin, Sudan

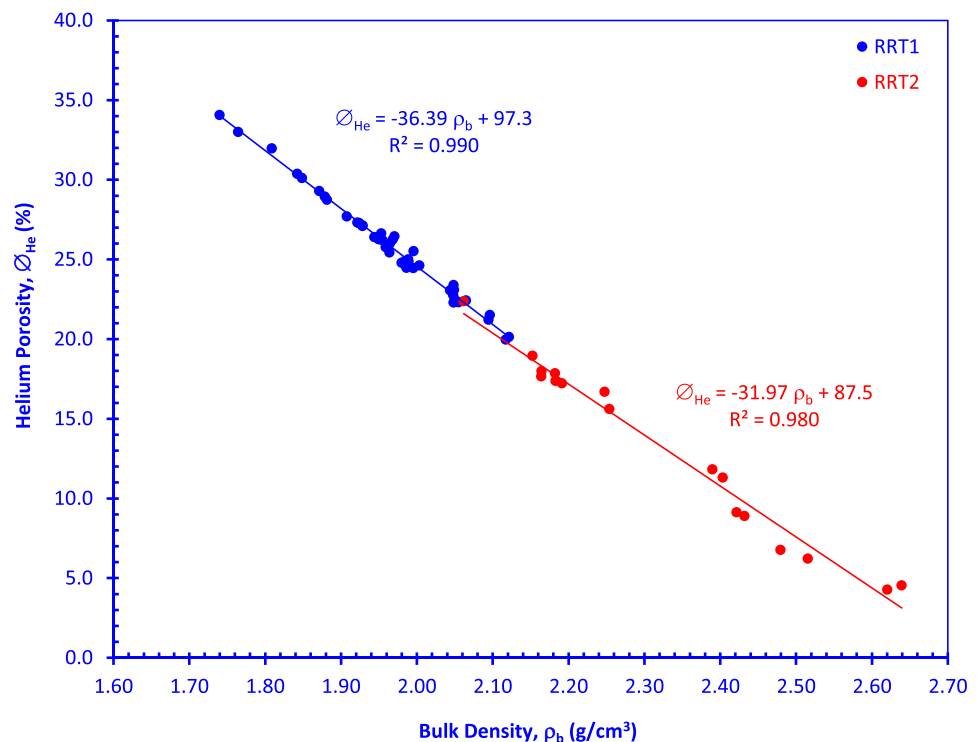


Fig. 7 Using the discrete rock type (DRT) method of Shenawi et al. (2007) as a successful tool to sort the studied samples into two rock types

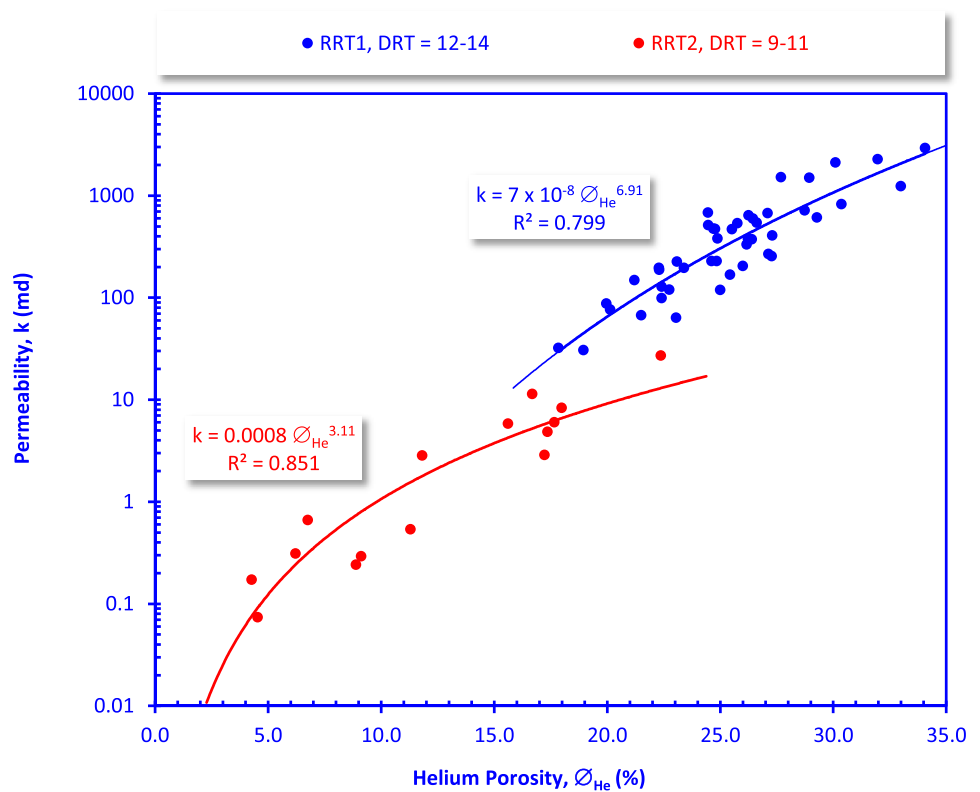
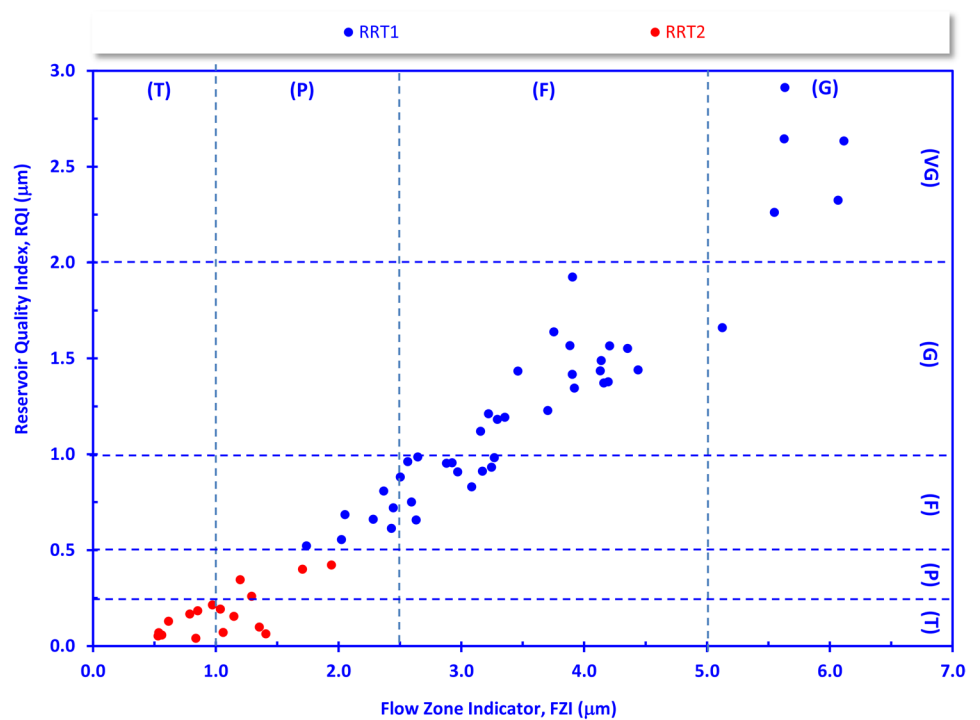


Fig. 8 Reservoir quality index (RQI) versus the flow zone indicator (FZI) as a tool to rank the studied samples. Ranks are classified following Nabawy et al. (2018b). T refers to tight reservoir quality, P, refers to poor reservoir, and F, G and VG refer to fair, good and very good quality, respectively.



permeability anisotropy in RRT2 Abu Gabra samples due to the presence of both secondary and depositional fabrics with horizontal shale streaks and a vertical micro fracture system (Fig. 4f).

Buckles’ plot

The bulk volume of water (BVW) is a critical parameter that explains the reservoir production of water rather than oil.

Fig. 9 Vertical permeability as a function of horizontal permeability, indicating the laminated and fractured samples

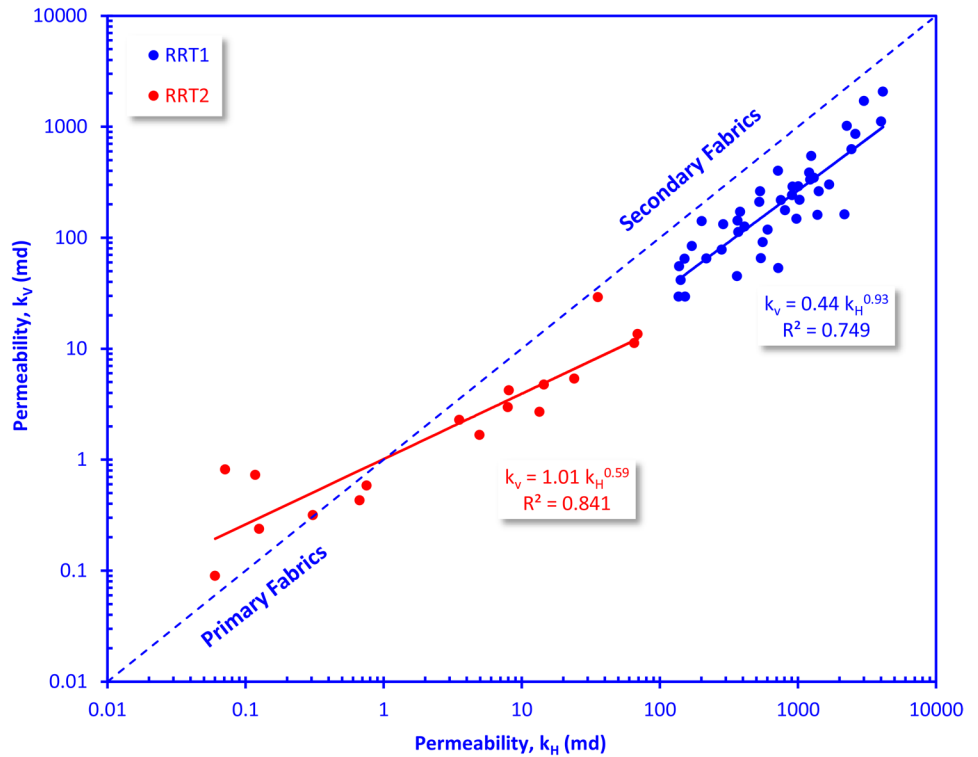
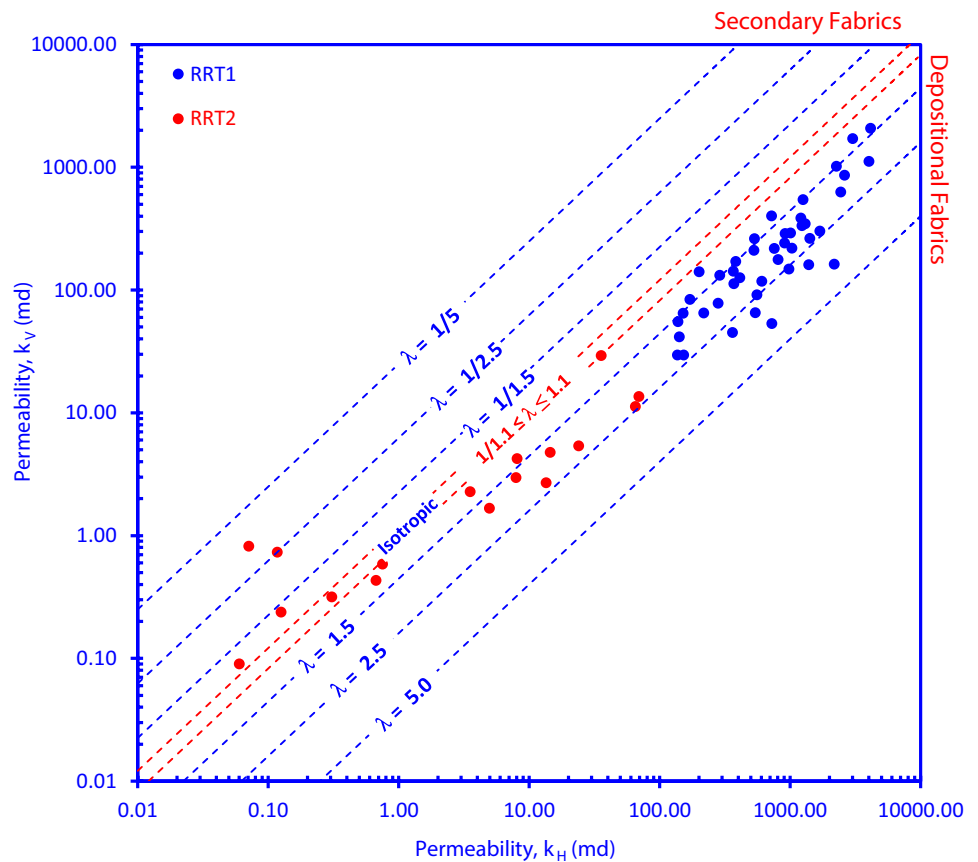


Fig. 10 Plotting the vertical and horizontal permeability as a function of their anisotropy (Nabawy et al. 2015). When $\lambda = 1.1-1.5$ samples are slightly depositional anisotropic fabrics; when $\lambda = 1.5-2.5$ samples are moderately depositional anisotropic; when $\lambda = 2.5-5.0$ samples are highly depositional anisotropic; when $\lambda > 5.0$ samples are very highly depositional anisotropic; when $\lambda = 1/1.1-1/1.5$ samples are slightly secondary anisotropic fabrics; when $\lambda = 1/1.5-1/2.5$ samples are moderately secondary anisotropic; when $\lambda = 1/2.5-1/5$ samples are highly secondary anisotropic; and when $\lambda < 1/5$ samples are very highly secondary anisotropic fabrics (Nabawy et al. 2015).



Low BVW values (0.005 for carbonates and 0.05 for clastic reservoir) indicate that a reservoir is at the irreducible water saturation (Sw_{irr}) point and will produce oil without water production, whereas the higher the BVW, the greater the water production (Asquith 1985). BVW can be calculated as follows (Buckles 1965; Holmes et al. 2009):

$$BVW = \phi \times Sw. \tag{11}$$

For the present study, plotting porosity as a function of Sw is supported by a set of BVW hyperbola to check the state of studied reservoir sequence, where a BVW value of 0.04 indicated the presence of some horizons Sw_{irr} and oil is produced without water, while increasing these values indicated production oil mixed with water and the highest values indicated only water production (Fig. 11). This plot indicates that, in spite of most of RRT1 samples having a water saturation value less than 0.40, RRT2 samples are characterized by Sw greater than 0.40 (Fig. 11). This can be attributed to the higher porosity values of RRT1 samples, i.e., greater ability of water to flow and to be produced during oil production (Nabawy et al. 2018a).

Reservoir characterization

Reservoir characterization is a specific process in which a much more precise characterization of additional specific parameters and properties is carried out to achieve reliable modeling that can predict future behavior. For the present

study, reservoir characterization includes estimates of Archie’s parameters (lithology factor a , and porosity exponent m) at ambient and overburden pressure, Sw_{irr} at overburden pressures of 200 psi, porosity and permeability at an overburden pressures up to 6000 psi pressure and relative permeability using different techniques.

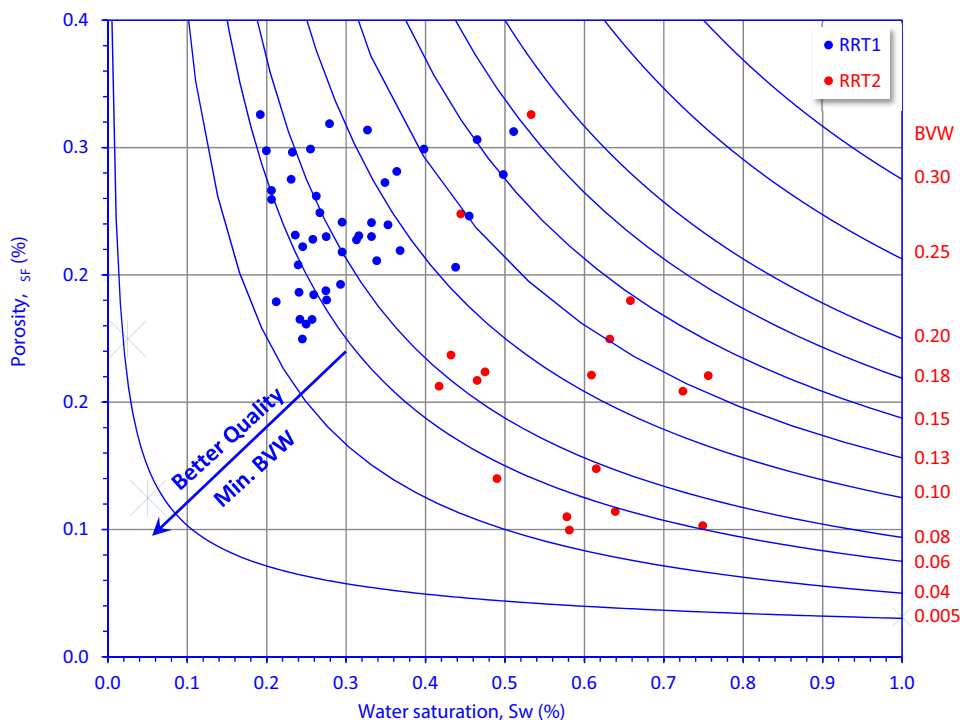
Impacts of mineral composition on FRF and Archie’s parameters

Although some authigenic clay content and iron oxides are present in the RRT2 samples (Fig. 4e, g), the measured values of the true formation resistivity factor (FRF) of the RRT2 samples are much higher than those of the RRT1 samples. This can be attributed to the high connectivity of pore spaces in the RRT1 samples with greater porosity and permeability values (Table 1).

Plotting FRF as a function of ϕ_w is required to estimate the Archie’s parameters (a and m) (Fig. 12). The plot in Fig. 10 indicates that a is greater than unity, while m is equal to 1.44 and 1.38 for RRT1 and RRT2, respectively, which may be attributable to the presence of calcareous cement (Fig. 4f, g) and argillaceous matrix (Fig. 4d, f). Decreasing the porosity exponent (m) may be another indication of good pore space connectivity. However, useful estimates of a , and m are essential to achieving accurate estimates of the original oil reserve and water saturation Nabawy et al. (2018b).

For the present study, Archie’s parameters were measured for RRT1 samples at 4300 psi of confining pressure.

Fig. 11 Buckles plot; porosity values as a function of the water saturation (BVW) (Buckles 1965; Holmes et al. 2009)



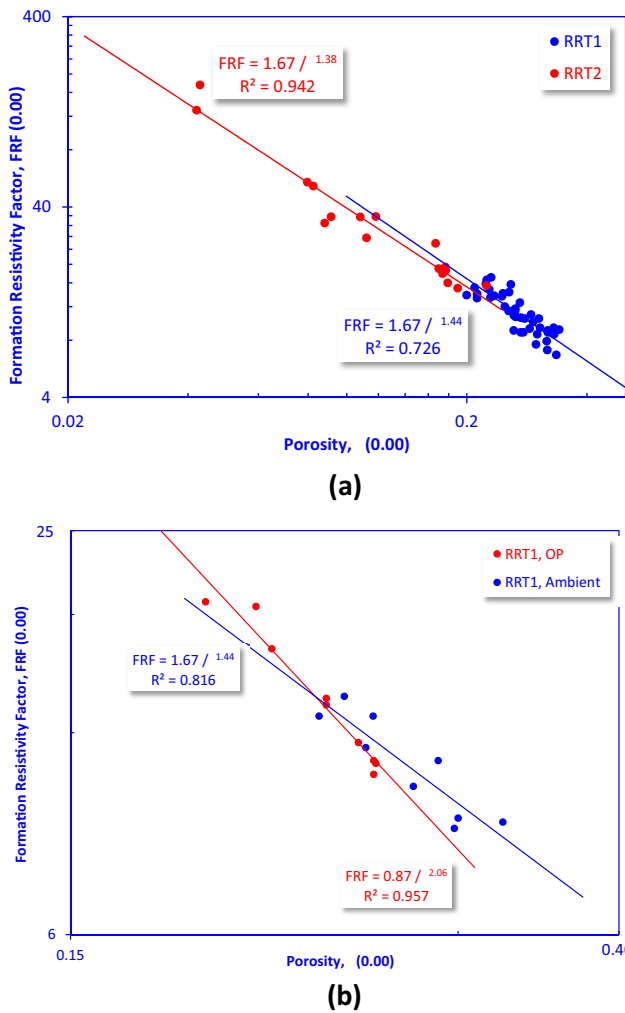


Fig. 12 Formation resistivity factor as a function of porosity to estimate the lithology factor a , and the porosity exponent m at: **a** ambient conditions, and **b** overburden pressure (OP) and ambient conditions

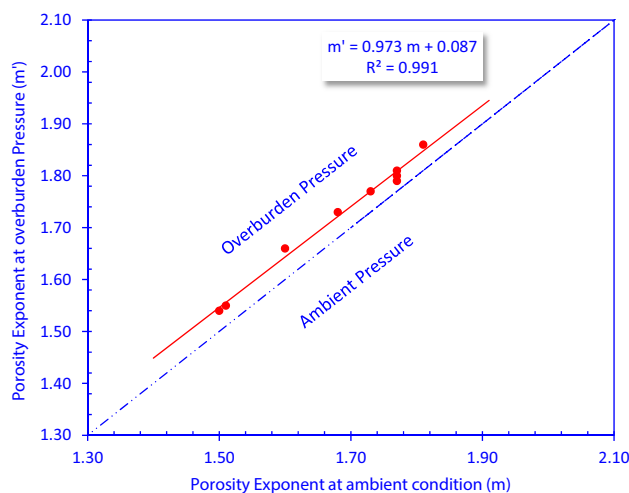


Fig. 13 Porosity exponent m at ambient conditions (a), and at overburden pressure (b) versus each other

Increasing the confining pressure increased the porosity exponent from 1.44 to 2.06. Increasing the porosity exponent is compensated for by reducing the lithology factor from 1.67 to 0.87 (Fig. 13). The porosity exponent of the RRT1 samples was estimated at a confining pressure for the samples group and also for each sample (forced-regression method, assuming $a = 1.0$). This indicates that for each sample, m increased slightly after applying a confining pressure on forced regression (av. $m = 1.68$, av. $m' = 1.72$, Fig. 13). The porosity exponent (m') of the plug samples at confining pressure can be estimated in terms of that measured at the ambient pressure (m) with very high reliability ($R^2 = 0.991$, Fig. 13).

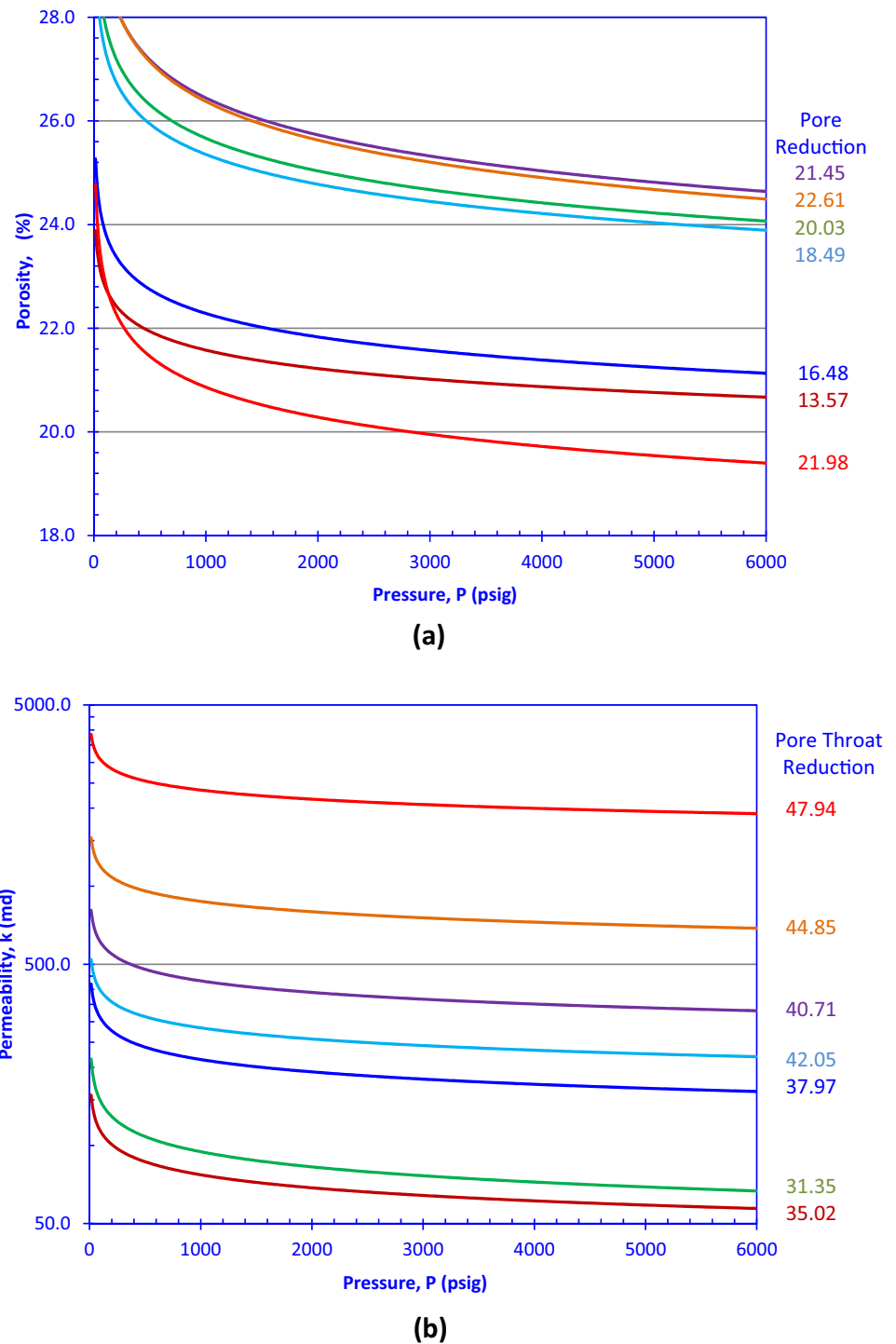
Irreducible water saturation (Sw_{irr}) and saturation exponent (n) estimation

Estimates of Sw_{irr} are essential for useful reservoir characterizations. For the present study, Sw_{irr} was measured using the porous plate method and an incremental increase in the applied pressure on fully saturated samples from 1 to 200 psi until Sw_{irr} was reached. This indicates that at 200 psi, the average Sw_{irr} for the RRT2 samples (av. $Sw_{irr} = 43.0\%$) is much higher than that for the RRT1 samples (average $Sw_{irr} = 18.3\%$). The minimum, maximum and average Sw_{irr} values for the Abu Gabra Formation (RRT2 samples) are much higher than those for the Bentiu Formation (RRT1 samples). This agrees with the fact that the RRT2 samples are dominated by a clay matrix that increases the total surface area of the rock sample due to their very fine flake sizes (Fig. 4f), and therefore retained more irreducible water saturation. However, the saturation exponent (n) is less than 2.0 for both RRT1 and RRT2 samples indicating the water-wet nature of the studied samples, i.e., the rock's ability to retain water rather than oil which is a preferable reservoir property.

Reservoir simulation

Reservoir simulation involves measuring porosity and permeability at varying confining pressures to reach the same reservoir pressure. Plotting porosity and permeability as a function of increasing pressure indicates that this increase in pressure causes reduction in pore volume and pore throat diameters. This can be achieved by measuring porosity and permeability at each incremental increase in confining pressure (Fig. 14). For the selected RRT1 samples, increasing the applied confining pressure caused pore a volume reduction (PR) between 13.57 and 22.61%, of average PR equals 19.3% at 6000 psi (Table 2, Fig. 14a). The impacts of increasing the confining pressure on the pore volume is much less than its effect on the pore throat reduction (PTHR) which can be estimated by measuring the permeability at each step of the

Fig. 14 Estimating the pore and pore throat reduction by plotting: **a** porosity, and **b** permeability as a function of the applied incremental pressure (Nabawy et al. 2018b)



applied confining pressure. The PTHR reaches 47.95%, with a minimum value of 31.34% (average PTHR = 39.62, Table 2, Fig. 14b). This can be explained by the sensitivity of the flow capacity as represented by permeability, to a reduction in pore throat diameter as a result of increased the confining pressure.

Relative permeability and wettability estimation

The relative permeabilities of the studied RRT1 for both oil and water are needed to estimate the mobility of oil and water in the different life-time steps of the producing well and are therefore important for estimating future

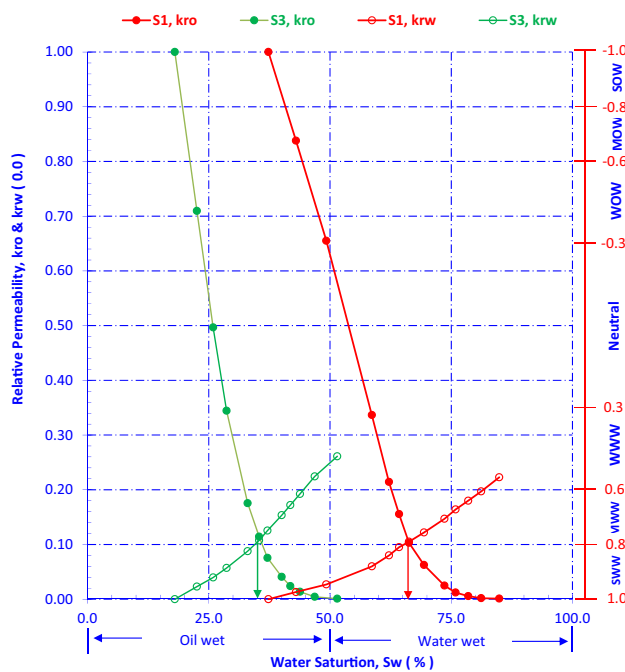


Fig. 15 Comparison between the common method for estimating wettability and the method proposed by Nabawy et al. (2018b)

oil and water production ratios. The relative permeability to water (k_{rw}) of the studied samples varies from 0.223 to 0.43, which indicates an ability to retain water rather than oil. The residual oil varies between 15.1 and 48.5%, while the Sw_{irr} varies from 18.0 to 37.3%. These values are more or less coincident with the Sw_{irr} values obtained from the porous plate method. This plot, which can be used to estimate wettability of the studied samples using a technique proposed by Nabawy et al. (2018b), indicated that, weak water to neutral wettability (Table 3). In addition, wettability was estimated using a common method (relative permeability intersection point RPIP, Fig. 15). From this plot it is clear that the studied samples are water to oil wet (Table 3).

Wettability was also estimated using the Amott technique. The Amott index varies from 0.409 to 0.689, which indicates weak to moderate water-wet and suggests that the method introduced by Nabawy et al. (2018b) while comparable to the Amott technique, is preferable due to its rapid turn around and low cost. The water wettability of the studied samples is also supported by the obtained saturation exponent which is typically less than 2 which indicates water or neutral wettability. The obtained wettability nature is preferable during oil production, which means that the reservoir will retain water and that oil will be free to flow.

Conclusions

Integrating the well log analysis, core data and sedimentological studies is a useful tool for discriminating the Bentiu-Abu Gabra sequences into a number of reservoir rock types (RRTs), hydraulic flow units (HFUs), and discrete rock types (DRTs). The well log data indicate that the average shale volume, effective porosity, and hydrocarbon saturation are 34.6%, 16.2%, and 65.1%, respectively, which are attractive values.

The petrographical studies, of the logged sequence, identified the studied sequence as; (1) quartz arenite, (2) quartz wacke, (3) subfeldspathic quartz arenite, and (4) subfeldspathic wacke. The quartz grains are the main component of the studied microfacies, whereas feldspars are present as subsidiary components. Alteration and dissolution of feldspars increased the pore volume but also increased the kaolinite content in the wacke microfacies. The reservoir quality of the studied microfacies was enhanced due to dissolution and leaching of both quartz grains and cement as well as fracturing, whereas compaction and pressure solution, cementation by silica and argillaceous material, and presence of authigenic minerals (kaolinite and siderite) reduced the reservoir quality. Pore spaces of these microfacies are represented mostly by intergranular, oversize pores, and microfractures. Dominance of kaolinite in some zones, particularly in the Abu Gabra Formation, indicated dominance of tropical continental settings to near-shore regions.

Petrophysically, these four microfacies can be summed up into two RRTs: RRT1 which is composed of quartz arenite and subfeldspathic quartz arenite, and RRT2 which is composed of quartz wacke, and subfeldspathic wacke. The reservoir quality of the RRT1, which is dominant through the Bentiu Formation, is superior to the quality of the RRT2 of Abu Gabra Formation. The reservoir quality index (RQI) and flow zone indicator (FZI) for RRT1 of the Bentiu Formation ($0.61 \leq RQI \leq 2.91 \mu\text{m}$, $2.37 \leq FZI \leq 6.12 \mu\text{m}$, and $12 \leq DRT \leq 14$, respectively, i.e., good-to-excellent reservoir quality) was superior to that for RRT2 of the Abu Gabra Formation, which exhibited tight-to-poor reservoir quality parameters with dominant good quality ($0.04 \leq RQI \leq 0.42 \mu\text{m}$, $0.53 \leq FZI \leq 1.94 \mu\text{m}$, $9 \leq RQI \leq 11 \mu\text{m}$, respectively, i.e., poor to fair reservoir quality).

The studied sequence can be classified into four HFUs, with approximately 95% of the flow capacity attributable to HFU-1 and -2, and both characterized by weak water to neutral wettability. Closure of pore throats by increasing pressure (6000psi) reached 47.9%, as indicated by measurements of permeability at high pressures.

Acknowledgements The authors would like to thank the Greater Nile Petroleum Operating Co. LTD. (GNPOC), North Sudan. Also, they

would like to thank those who offered help during sample preparation, measurements and data interpretation. The authors extend their sincere appreciation to Prof. Dr. Aref Lashin at King Saud University in Saudi Arabia for his technical support and help in revising the first draft paper. The authors express their appreciation and acknowledgement to the editor-in-Chief Prof. Dr James W. LaMoreaux, and the anonymous reviewers for their constructive comments that greatly reformulated the present paper.

Compliance with ethical standards

Conflict of interest The authors hereby declare that they have no conflict of interest, where they didn't receive fund or grant to cover the present study. The authors confirm that they didn't receive a speaker honorarium from any companies and don't own stock in companies. In addition, all the authors are not committee members in any organizations that may causes conflict of interest.

References

- Abdalla YM, Michael JP, William AA (2002) Petroleum maturation modelling, Abu Gabra Sharaf area, Muglad Basin, Sudan. *J. Afr. Earth Sci.* 35:331–344
- Abdelhakam EM, Ali SM (2008) Stratigraphy and tectonic evolution of the oil producing horizons of Muglad Basin. *Sudan J Sci Technol* 9:1–9
- Abed AA (2014) Hydraulic flow units and permeability prediction in a carbonate reservoir, Southern Iraq from well log data using non-parametric correlation. *Int J Enhanced Res Sci Technol Eng* 3(1):480–486
- Amaefule JO, Altunbay M, Tiab D, Kersey DG, Keelan DK (1993) Enhanced reservoir description: using core and log data to identify hydraulic (flow) units and predict permeability in uncored intervals/wells. SPE 26436. In: Presented at the annual technical conference and exhibition, Houston, TX, pp 3–6
- Archie GE (1942) The electric resistivity logs as an aid in determining some reservoir characteristics. *Trans Am Int Mech Eng* 146:54–62
- Asquith GB (1985) Handbook of log evaluation techniques for carbonate reservoirs. Methods in exploration Series no. 5, The American Association of Petroleum Geologists, Tulsa, Oklahoma, USA, 47.
- Buckles RS (1965) Correlating and averaging connate water saturation data. *J Can Petrol Technol* 9(1):42–52
- Corbett PWM, Potter DK (2004) Petrotyping: a base map and Atlas for navigating through permeability and porosity data for reservoir comparison and permeability prediction. In: International symposium of the society of core analysts. SCA2004-30, pp 1–12
- David C, Bertauld D, Dautriat J, Sarout J, Menéndez B, Nabawy BS (2015) Detection of moving capillary front in porous rocks using X-ray and ultrasonic methods. *Front Phys* 3(A053):1–14
- De Ros LF, Goldberg K (2007) Reservoir petrofacies: a tool for quality characterization and prediction, part 1. In: AAPG, annual convention and exhibition, Long Beach, abstracts volume
- Dou L, Zhang Z, Cheng D (2006) Control of regional seal on oil accumulations in the Muglad Basin, Sudan. *Acta Petrol Sin* 27(3):22–26
- Dou L, Cheng D, Li Z, Zhang Z, Wang J (2013) Petroleum geology of the Fula subbasin, Muglad basin, Sudan. *J Petrol Geol* 36:43–59
- Dykstra H, Parsons RL (1950) The prediction of oil recovery by water flooding. Secondary recovery of oil in the United States, 2nd edn. API, Washington, DC, pp 160–174
- El Sharawy MS, Nabawy BS (2018) Determining the porosity exponent and lithology factor for sandstones and their control by overburden pressure: a case study from the Gulf of Suez, Egypt. *Am Assoc Petrol Geol Bull* 102(9):1893–1910
- El Hassan WM, Farwa AG, Awad MZ (2017) Inversion tectonics in central Africa rift system: evidence from the Heglig field. *Mar Petrol Geol* 80:293–306
- El Sawy MZ, Abuhagaza AA, Nabawy BS, Lashin A (2020) Rock typing and hydraulic flow units as a successful tool for reservoir characterization of Bentiu–Abu Gabra sequence, Muglad basin, southwest Sudan. *J Afr Earth Sci* 171:103961
- Elgendy NTH, Abuamarah BA, Nabawy BS, Ghrefat H, Kassem OMK (2020) Pore fabric anisotropy of the Cambrian–Ordovician Nubia sandstone in the Onshore Gulf of Suez, Egypt: a surface outcrop analog. *Nat Resour Res* 29(2):1307–1328
- Fairhead JD (1988) Mesozoic plate tectonic reconstructions of the Central South Atlantic Ocean: the role of the West and Central African rift system. *Tectonophysics* 155(1):181–191
- Holmes M, Holmes D, Holmes A (2009) Relationship between porosity and water saturation: methodology to distinguish mobile from capillary bound water. In: AAPG annual convention, Denver, Colorado June 7–10: article 110108
- Kassab MA, Abdou AA, El Gendy NH, Shehata MG, Abuhagaza AA (2017a) Reservoir characteristics of some Cretaceous sandstones, North Western Desert, Egypt. *Egypt J Petrol* 26:391–403
- Kassab MA, Abu Hashish MF, Nabawy BS, Elnaggar OM (2017b) Effect of kaolinite as a key factor controlling the petrophysical properties of the Nubia sandstone in central Eastern Desert, Egypt. *J Afr Earth Sci* 125:103–117
- Lowell JD, Genik GJ (1972) Sea floor spreading and structural evolution of southern Red Sea. *AAPG Bull* 56:247–259
- Maglio-Johnson T (2000) Flow unit definition using petrophysics in a deep water turbidite deposit, Lewis Shale, Carbon County, Wyoming. Publishing M.Sc. thesis, Colorado School of Mines
- Makeen YM, Abdullah WH, Pearson MJ, Hakimi MH, Elhassan OMA, Hadad YT (2016) Thermal maturity history and petroleum generation modelling for the Lower Cretaceous Abu Gabra Formation in the Fula Sub-basin, Muglad Basin, Sudan. *Mar Petrol Geol* 75:310–314
- McHargue TR, Heidrick JL, Livingstone JE (1992) Tectonostratigraphic development of the interior Sudan rifts, Central Africa. *Tectonophysics* 213:187–202
- Mousa DA, Abdou AA, El Gendy NH, Shehata MG, Kassab MA, Abuhagaza AA (2014) Mineralogical, geochemical and hydrocarbon potential of subsurface Cretaceous shales, Northern Western Desert, Egypt. *Egypt J Petrol* 23(1):67–78
- Nabawy BS (2018) Impacts of fossil anisotropy on the electric and permeability anisotropy of highly fossiliferous limestone: a case study. *Mar Geophys Res* 39(4):537–550
- Nabawy BS, El Sharawy MS (2015) Hydrocarbon potential, structural setting and depositional environments of Hammam Faraun Member of the Belayim Formation, Southern Gulf of Suez, Egypt. *J Afr Earth Sci* 112:93–110
- Nabawy BS, Sediek KN, Nafee SA (2015) Pore fabric assignment using electrical conductivity of some Albian–Cenomanian sequences in north Eastern Desert, Egypt. *Arabian J Geosci* 8(8):5601–5615
- Nabawy BS, Basal AMK, Sarhan MA, Safa MG (2018a) Reservoir zonation, rock typing and compartmentalization of the Tortonian–Serravallian sequence, Temsah Gas Field, offshore Nile Delta, Egypt. *Mar Petrol Geol* 92:609–631
- Nabawy BS, Rashed MA, Mansour AS, Afify WSM (2018b) Petrophysical and microfacies analysis as a tool for reservoir rock typing and modeling: Rudeis Formation, off-shore October Oil Field, Sinai. *Ma Petrol Geol* 9:260–276
- Nabawy BS, Elgendy NTH, Gazia MT (2020) Mineralogic and diagenetic controls on reservoir quality of paleozoic sandstones, Gebel El-Zeit, North Eastern Desert, Egypt. *Nat Resour Res* 29(2):1215–1238

- Pettijohn FJ, Potter PE, Siever R (1987) *Sand and Sandstone*. Springer, Berlin
- Qiao J, Liu L, An F, Xiao F, Wang Y, Wu K, Zhao Y (2016) Hydrocarbon potential evaluation of the source rocks from the Abu Gabra Formation in the Sufyan Sag, Muglad Basin, Sudan. *J Afr Earth Sci* 118:301–312
- Raymond LA (2002) *Petrology, the study of igneous, sedimentary and metamorphic rocks*, 2nd edn. Appalachian State University, Boone
- Schull TJ (1988) Rift basins of interior Sudan: petroleum exploration and discovery. *AAPG Bull* 72:1128–1142
- Serra O (1988) *Fundamentals of well-log interpretation*. 1. The acquisition of logging data, 3rd edn. Elsevier, Amsterdam
- Shenawi SH, White JP, Elrafie EA, Kilany KA (2007) Permeability and water saturation distribution by lithologic facies and hydraulic units: a reservoir simulation case study. SPE, SPE-105273-MS
- Teh WJ, Willhite GP, Doveton JH (2012) Improved reservoir characterization using petrophysical classifiers within electrofacies. SPE, SPE-154341-PP
- Tiab D, Donaldson EC (1996) *Petrophysics, theory and practice of measuring reservoir rock and fluid transport properties*. Gulf Publ. Co., Houston, pp 205–220

Publisher's Note Springer Nature remains neutral with regard to jurisdictional claims in published maps and institutional affiliations.